Atmos. Chem. Phys. Discuss., 15, 25503–25545, 2015
www.atmos-chem-phys-discuss.net/15/25503/2015/
doi:10.5194/acpd-15-25503-2015

Atmospheric Chemistry and Physics Discussions

Observations of high droplet number concentrations in Southern Ocean boundary layer clouds

T. Chubb[1], Y. Huang[1,2], J. Jensen[3], T. Campos[3], S. Siems[1,2], and M. Manton[1]

[1]School of Earth, Atmosphere and Environment, Monash University, VIC 3800, Australia
[2]Australian Research Council (ARC) Centre of Excellence for Climate System Science, Monash University, VIC 3800, Australia
[3]NCAR Research Aviation Facility, 10802 Airport Court Rocky Mountain Metropolitan Airport Broomfield, CO 80021, USA

Received: 31 August 2015 – Accepted: 2 September 2015 – Published: 17 September 2015

Correspondence to: T. Chubb (thomas.chubb@monash.edu)

Published by Copernicus Publications on behalf of the European Geosciences Union.

Abstract

Data from the standard cloud physics payload during the NSF/NCAR High-performance Instrumented Airborne Platform for Environmental Research (HIAPER) Pole-to-Pole Observations (HIPPO) campaigns provide a snapshot of unusual wintertime microphysical conditions in the boundary layer over the Southern Ocean. On 29 June 2011, the HIAPER sampled the boundary layer in a region of pre-frontal warm air advection between 58 and 48° S to the south of Tasmania. Cloud droplet number concentrations were consistent with climatological values in the northernmost profiles but were exceptionally high for wintertime in the Southern Ocean at 100–200 cm^{-3} in the southernmost profiles. Sub-micron ($0.06 < D < 1\,\mu m$) aerosol concentrations for the southern profiles were up to 400 cm^{-3}.

Analysis of back trajectories and atmospheric chemistry observations revealed that while conditions in the troposphere were more typical of a clean remote ocean airmass, there was some evidence of continental or anthropogenic influence. However, the hypothesis of long range transport of continental aerosol fails to explain the magnitude of the aerosol and cloud droplet concentration in the boundary layer. Instead, the gale force surface winds in this case (wind speed at 167 m above sea level was $> 25\,m\,s^{-1}$) were most likely responsible for production of sea spray aerosol which influenced the microphysical properties of the boundary layer clouds. The smaller size and higher number concentration of cloud droplets is inferred to increase the albedo of these clouds, and these conditions occur regularly, and are expected to increase in frequency, over windy parts of the Southern Ocean.

1 Introduction

The remote Southern Ocean (SO; poleward of 45° S) has received recent attention due to substantial biases in both reanalysis and climate simulations associated with clouds (Meehl et al., 2007; Trenberth and Fasullo, 2010). In this pristine environment,

ACPD
15, 25503–25545, 2015

cloud properties may be sensitive to relatively small changes in aerosol concentrations, whether from anthropogenic or natural sources, but there has been a distinct lack of in-situ microphysical observational campaigns in this region in recent years. High latitude ocean-atmosphere interactions and processes have been identified as a key research frontier by the NSF Advisory Committee for Geosciences (2014).

The pristine environment of the SO raised questions about cloud droplet number concentration (N_C) and droplet sizes there in the early 1990s. Boers et al. (1996); Boers and Krummel (1998), and Boers et al. (1998) considered N_C within, and cloud condensation nuclei (CCN) concentrations below, SO boundary layer clouds in "baseline" conditions (with an airmass history far from continental Australia) during the First Aerosol Characterization Experiment (ACE-I, November to December 1995) and the two phases of the Southern Ocean Cloud Experiment (SOCEX-I, July 1993; SOCEX-II, February 1995). In wintertime, N_C was found to be low, at typically 10–40 cm^{-3} for clouds of up to 300 m deep, compared to summertime values of 50–180 cm^{-3}. A caveat with the lowest wintertime N_C values of that study is that they were highly correlated with the cloud liquid water content, suggesting that clear air may have been mixed into those samples.

Seasonal differences in N_C during the SOCEX experiments were attributed to oxidation products of oceanic dimethylsulphide (DMS) acting as CCN, due to seasonal variation in the productivity of the ocean (Boers et al., 1998). At the time it was widely hypothesized that DMS-derived particulates made up the bulk of all sub-micrometer particles (Charlson et al., 1987), which linked ocean productivity to cloud albedo and thus global climate through the so-called "CLAW" hypothesis. However, a review of two decades of subsequent research suggested that the evidence for each of the stages in this mechanism was rather weak (Quinn and Bates, 2011), and that sea spray aerosol (SSA) comprises a substantial fraction of the marine boundary layer CCN concentration.

The HIAPER Pole-to-Pole Observations flights (HIPPO; Wofsy, 2011) were not dedicated cloud physics experiments but have nevertheless provide some new data at high

ACPD
15, 25503–25545, 2015

latitudes over the SO. Chubb et al. (2013) examined two SO flights that encountered low-altitude cloud (i.e. below 2 km) across a broad latitude range. Direct N_C observations were only available on one of those flights, which took place in the month of April, and ranged from 30–50 cm^{-3} in weakly convective stratocumulus cloud in the cold air sector of an extratropical cyclone at latitudes around 59° S, to 80–120 cm^{-3} in a region of homogeneous stratiform cloud in moderate south-westerly flow between 62–67° S. Broadly speaking, these values were in line with those from ACE-I and the SOCEX experiments.

Cloud particle effective radius r_e and optical thickness τ are standard retrievals (e.g. Nakajima and King, 1990) that may be performed with radiance data from the Moderate Resolution Imaging Spectroradiometer (MODIS; Salomonson et al., 1989). Bennartz (2007) used two and a half years of Aqua MODIS retrievals to calculate N_C over remote oceanic regions. N_C values for the Southern Hemisphere oceans (equatorward of 60° S) were 40–67 cm^{-3}, compared to 64–89 cm^{-3} for the Northern Hemisphere. The estimated frequency of drizzle (based on empirical relationships with N_C and cloud geometric thickness) was substantially higher in the Southern Hemisphere oceans. A limitation in the use of these retrievals at high latitudes, which was not considered by Bennartz (2007), is the solar angle, which must be greater than about 65° to be reliable (Grosvenor and Wood, 2014). In wintertime, it is virtually impossible to perform robust r_e retrievals over the SO.

The primary mechanism of SSA production is the bursting of small bubbles at the sea surface within breaking wave crests, or whitecaps (Day, 1964). The "film drop" particles produced are typically in the radius range of 0.01–1 µm, remain suspended for long periods, and form the dominant contribution to marine SSA number concentration (Lewis and Schwartz, 2004, ch. 4). Larger particles can be formed in lower concentrations by "jet" and "spume" mechanisms, but these tend to fall to the sea surface on time scales of seconds to hours and may not contribute substantially to CCN number concentrations.

ACPD
15, 25503–25545, 2015

In spite of the intuitive link between wind speed and SSA concentration, which has long been recognized (Woodcock, 1953), the case for a formulation based on wind speed alone is mixed. SSA production flux per whitecap area is typically assumed to be independent of wind speed, permitting estimates based on fractional whitecap area (W). However, W can vary by an order of magnitude for the same wind speed (Lewis and Schwartz, 2004, ch. 3), and the underlying uncertainties in the production fluxes are large (de Leeuw et al., 2011). In spite of this, a relationship between the logarithm of SSA concentration (N_{SSA}) and the local wind speed is typically assumed. Several studies (e.g. Marks, 1990; O'Dowd and Smith, 1993; Nilsson et al., 2001) report very good agreement with this formulation, but during ACE-I, other investigators have reported little or no correlation of N_{SSA} with wind speed (Bates et al., 1998; Covert et al., 1998; Berg et al., 1998). More recently, (Blot et al., 2013) presented observations of N_{SSA} made in the unpolluted south-eastern Pacific during the VOCALS (Variability of the American Monsoon Systems (VAMOS) Ocean-Cloud-Atmosphere-Land Study) campaign. These data, recorded over 1000 km along the 20° S meridian, showed only a weak relationship to wind speeds up to about 12 m s^{-1}. The authors concluded that other factors, especially local precipitation history, may play an important role in determining SSA concentrations.

High aerosol concentrations over the SO – an important topic for this paper – could also be caused by long range transport of aerosol from the Australian continent. Using back trajectory analysis coupled with radon and condensation nuclei (CN) concentration observations, Downey et al. (1990) found that long range transport could explain up to 25 % of the variance of radon concentration, which is a good proxy for "land contact", at Macquarie Island. CN concentrations reached values above 1000 cm^{-3} for short intervals while trajectories were of continental origin, but the trajectory statistics used ("hours of land contact" and "time since land contact") showed very poor, and even negative, correlation to CN concentrations. This was attributed to non-uniformity of CN sources on the continent and processes acting as sinks and sources over the ocean (neither of which affect radon concentration).

ACPD
15, 25503–25545, 2015

This paper focuses on some observations from a single flight over the SO in winter during the 4th HIPPO campaign (HIPPO-4), which we selected because cloud droplet and aerosol concentrations were considerably higher than expected in a region that was more than 1500 km from the nearest potential pollution sources. The main hypothesis addressed by this paper is that these observations can be attributed to high SSA production due to very strong low-level winds with the approach of a strong cold front. Our objectives are firstly to verify and analyze the in-flight microphysics observations, which were not intensive due to their secondary importance for the HIPPO missions, and secondly to investigate the alternative hypothesis that long-range transport of continental/anthropogenic aerosols influenced microphysical conditions.

2 Methodology and data

With the primary objective of conducting a global survey of climatically important aerosols and trace gases, the NSF/NCAR HIAPER (a high-performance research aircraft based on a Gulfstream-V jet), conducted five global transects in different seasons between 2009 and 2011 for the HIPPO campaigns (Wofsy, 2011).

The primary dataset used to perform the analyses in this paper was the "Low Rate (1 Hz) Navigation, State Parameter and Microphysics Flight-Level Data" product (Romashkin, 2012) prepared by the NCAR Research Aviation Facility (RAF). In addition, we used one-second data from additional instrumentation, which was processed by various HIPPO investigators separately from the flight-level data (see below). These data formed the basis for the median-filtered "Merged 10 s Meteorology, Atmospheric Chemistry, and Aerosol Data" product (Wofsy et al., 2012), which has been used in many of the publications resulting from the HIPPO campaigns.

ACPD
15, 25503–25545, 2015

2.1 Flight overview

During daylight hours of 28–29 June 2011 (solar time), the HIAPER flew from Christchurch (New Zealand), to Hobart (Australia) via a way-point at 58° S, due south of Hobart. The Mean Sea Level Pressure (MSLP) analysis for 00:00 UTC 29 June 2011 (Fig. 1) shows a remarkably strong blocking anticyclone with a high-pressure center of 1042 hPa over the Tasman Sea. A mature, decaying frontal system was approaching from the west, with a secondary wave anomaly located at about 48° S, 130° E. This synoptic pattern generated a strong south-westerly pressure gradient in the pre-frontal airmass, with ERA-Interim wind speeds at 950 hPa in excess of 20 m s^{-1} associated with strong poleward warm air advection.

The Aqua satellite passed overhead at 03:45 UTC, while the HIAPER was mid-flight. MODIS retrievals show widespread boundary layer clouds with cloud top temperature (CTT) of 270 to 280 K underneath the blocking high (Fig. 2). A complex of multilayer cloud, with CTT in the range of 220–240 K, resided in the pre-frontal stream overlying the boundary layer cloud. In the vicinity of the secondary wave anomaly, the high level cloud band was broken, permitting retrievals of the boundary layer cloud beneath, which appeared to be consistent with the cloud well ahead of the frontal band.

The aircraft performed four descent/ascent profiles between 9000 and 160 m above sea level (a.s.l.) while in transit from the southernmost point to Hobart, which we discuss in reverse order (north to south) below. The locations of the short leg at about 160 m a.s.l. between the descent and ascent profiles are shown in Fig. 2, and imagery from the forward facing camera showing cloud top conditions are provided in Fig. 3. Conditions were quite varied between the profiles, with profiles 3 and 4 occurring close to the location of the synoptic front, and profiles 1 and 2 in pre-frontal conditions. In all but profile 1, there was some cirrus cloud well above the maximum altitude reached in the profiles.

ACPD
15, 25503–25545, 2015

2.2 HIPPO basic cloud physics instrumentation

Basic cloud microphysics instruments were operated in addition to the primary payload instrumentation, including:

- *Particle Measurement Systems 2-D Cloud Imaging Probe (2DC).* Precipitation particles larger than about 50 µm can be imaged by optical array probes such as the 2DC. The instrument returns particle statistics in the form of a size distribution histogram with 64 bins between 12.5 and 1600 µm as well as individual particle images. Here, as for most applications of the 2DC, we only use particles with diameters larger than 62.5 µm to determine drizzle drop number concentrations and rain rates (no ice was observed in the boundary layer clouds).

- *Droplet Measurement Technologies (DMT) Cloud Droplet Probe (CDP).* The CDP operates by illuminating individual droplets with a laser beam and measuring the intensity of the forward-scattered light over angles between 4 and 12° (Lance et al., 2010), and sizes them with a multi-channel analyzer. The instrument returns a particle size distribution over 30 bins between 2.0 and 50 µm at 1 Hz. Particle number concentration (N_C) and liquid water content (ρ_L; g m^{-3}) are subsequently derived from the size distribution. The CDP sizing was calibrated using glass beads of known sizes in Boulder, CO, prior to the commencement of HIPPO-4. Subsequently to the HIPPO missions, the CDP had its true sample area evaluated through a laboratory beam mapping by the manufacturer in June 2015.

- *DMT Ultra High Sensitivity Aerosol Spectrometer (UHSAS).* The UHSAS measures sizes of aerosol particles between 60 and 1000 nm based on light scattering (Cai et al., 2008). The instrument was calibrated using polystyrene latex beads of known sizes prior to HIPPO-4. We designate the total particle concentration measured by the UHSAS as N_U in this paper.

ACPD
15, 25503–25545, 2015

Additionally, there are a number of basic thermodynamic and inertial observations used in this paper, and real-time forward digital camera imagery was available for all flights.

We partitioned the data by liquid water content, using $\rho_L < 0.01\,\mathrm{gm}^{-3}$ for "probably clear" samples, needed for ensuring that the UHSAS observations were robust; and $\rho_L > 0.05\,\mathrm{gm}^{-3}$ for "confident cloudy" samples, for calculating N_C from the CDP data. Similar thresholds are commonly used to discriminate between clear and cloudy samples (e.g. Wood and Field, 2011; Boutle et al., 2014) when high-rate data is unavailable (as in this case). Our study differs by using two thresholds to more selectively discriminate between cloudy and clear air.

2.3 HIPPO trace gas and aerosol instrumentation

To address the possibility that the high aerosol concentrations observed in the boundary layer are due to long range transport of pollution from the Australian continent, we used atmospheric chemistry collected during the flight:

- *DMT Single Particle Soot Photometer (SP2).* The presence of black carbon (BC), or soot, indicates combustion, and is an excellent tracer for anthropogenic aerosol sources. The SP2 measures the incandescence temperature of particles illuminated by a laser beam (Schwarz et al., 2006). BC data acquired in clouds were removed from the HIPPO dataset based on SP2 internal diagnostics, the 2DC and CDP, and the hot-wire liquid water sensor.

- *AeroLaser Vacuum Ultra Violet (VUV) resonance fluorescence instrument.* Carbon monoxide (CO) is another useful indicator of combustion, but there are also natural marine sources. The VUV operates on the principle of CO fluorescence in the 160–190 nm wavelength range upon excitation with ultra violet light at 150 nm. The technology is relatively mature and has been employed on aircraft platforms for over a decade (Gerbig et al., 1999).

ACPD
15, 25503–25545, 2015

Unfortunately, there was no compositional analysis of aerosols performed apart from the presence of BC. In principle, this leaves open the possibility of elevated N_U values due to continental (mineral) dust in the absence of CO or BC, as anthropogenic aerosol emissions are almost exclusively produced in conjunction with combustion. We explore this possibility further in Sect. 4.4.

2.4 Calculation of back trajectories

We used the Hybrid Single Particle Lagrangian Integrated Trajectory Model (HYSPLIT; Draxler and Hess, 1998) to calculate back trajectories via the Air Resources Laboratory (ARL) portal (http://www.arl.noaa.gov/HYSPLIT.php). The meteorological data selected to run the calculations was based on output from the U.S. National Weather Service's National Centers for Environmental Prediction (NCEP) Global Data Assimilation System (GDAS). The ARL processes and archives this output as a 3 hourly, global, one degree latitude-longitude dataset on mandatory pressure levels (21 levels between 1000 and 1 hPa), and makes it available on the HYSPLIT portal.

Back trajectories were initialized along the flight path where the HIAPER was within the boundary layer cloud in profiles 1–4, at levels of 500 (within the boundary layer), 1500 (just above the boundary layer top) and at a third height between 3000 and 4500 m a.s.l., selected based on features of the atmospheric chemistry data. The initialization time for each location was the closest hour to the time that the HIAPER was in cloud, and the total duration of the trajectories calculated was 72 h. To account for synoptic-scale vertical motion, we used modeled vertical velocities instead of assuming isobaric or isentropic motion.

In order to test the sensitivity of the trajectory calculations to some of the uncertainties identified above, we used an ensemble approach, where 26 additional trajectories were calculated in addition to the "deterministic" one. These were initialized at horizontal perturbations of Δx and Δy of one grid point (one degree), and $\Delta\sigma$ of 0.01 (about 250 m), which is the standard configuration recommended by the ARL portal.

ACPD
15, 25503–25545, 2015

3 Analysis of flight data

3.1 Basic thermodynamic observations

Figure 4 shows thermodynamic observations from each of the descending profiles from the 1 Hz dataset. The values for the ascending profiles were not substantially different, except that the HIAPER ascended through a cloud-free patch during profile 2. Profile 1, the northernmost and furthest ahead of the synoptic front, is a classic example of a well-mixed marine boundary layer capped with stratocumulus cloud. There was a strong virtual potential temperature (θ_v) inversion at cloud top of about 6 °C. The height of the inversion was about 1150 m, and the temperature at cloud top (CTT), just below the inversion, was about 2 °C, so there was no supercooled liquid cloud anywhere in the layer. Immediately above cloud top the air was very dry, but below cloud base water vapor was well-mixed with a specific humidity (q_v) of about 6 g kg^{-1}. The cloud layer itself was about 400 m deep, and in cloud, ρ_L was near-adiabatic with peak values of around 0.60 g m^{-3} at cloud top. This environment appears to be typical for stratocumulus conditions. Horizontal winds were from the northwest and decreased from 20 to 15 m s^{-1} through the boundary layer, with little directional change at lower levels.

Profile 2 shares a number of features with the classic example of profile 1, but most notably the θ_v profile is more complex. The boundary layer top (main θ_v increase) was at about 1130 m a.s.l. and was coincident with the cloud top, with a temperature of 2 °C. Above this was a cloud-free intermediate layer of about 200 m, with a weaker θ_v increase at 1320 m a.s.l. At cloud top ρ_L was as high as 0.6 g m^{-3}, and was approximately adiabatic in the upper 300 m of the cloudy layer. Below this there was a layer about 250 m deep with relatively consistent values of $\rho_L \simeq 0.25$ g m^{-3}, which we interpret as a cumulus cell rising into the stratocumulus deck above. Winds below cloud displayed a more or less typical Ekman spiral with a directional shift of about 15° and decrease of 5 m s^{-1} between the cloud base and the lowest flight level.

ACPD
15, 25503–25545, 2015

The intermediate layer between cloud top and the free troposphere had characteristics similar to the "buffer layer" described by Russell et al. (1998), with q_v of similar value to within the boundary layer, but decreasing sharply above the buffer layer. The wind speed was about 5 m s^{-1} lower within this layer than within the boundary layer below or the free troposphere above, but there was no significant directional change. Such intermediate layers were typically identified between the boundary layer and free troposphere in ACE-I. Hande et al. (2012b) identified buffer layers in about 33 % of all Macquarie Island (54.62° S, 158.85° E) soundings, so while profile 2 may differ from the classic structure of profile 1, it is considered to be common for the SO.

Profiles 3 and 4 are quite different in nature to the more typical profiles discussed above. Both profiles had a boundary layer depth of about 1250 m, with a 0.5 °C inversion in profile 3 and about 4 °C in profile 4.

The cloud that was observed in these profiles occurred in the lower levels where the temperature was exclusively above 0 °C. Conditions were considerably more stably stratified than for profiles 1 and 2 (θ_v increased with height but was still conditionally unstable), implying that the boundary layer was less well-mixed. The cloud was coincident with high wind shear magnitude, in association with an Ekman spiral below 600 m a.s.l., especially in profile 4. While the cloud fields visually resembled stratocumulus layers (see Fig. 3), peak ρ_L values were not located near cloud top as they were in profiles 1 and 2. The cloud field in profile 3 was fairly continuous and flat-topped, but some gaps could be identified during the descent. Cloud top was less well defined in profile 4, with larger broken regions, and highly variable ρ_L values suggesting that clear air was sampled between cloud patches. Patchy mid-level cloud layers were also sampled between 2500 and 4500 m a.s.l. for both of these profiles, but some of these were beyond the altitude range plotted in Fig. 4.

The boundary layer wind speeds for profiles 3 and 4 were very high. Winds of 29 m s^{-1} in profile 3 were observed at around 500 m a.s.l. Above this altitude, winds receded slightly to about 25 m s^{-1} at 1000 m a.s.l. (the boundary layer top), then increased with height to a maximum of about 33 m s^{-1} in the lower free troposphere. The

ACPD
15, 25503–25545, 2015

winds at the lowest level of flight were at least 23 m s^{-1}, which is likely in the range for spume production at the ocean surface. Profile 4 was windier still, with peak wind speeds in the boundary layer of nearly 35 m s^{-1}, and the wind speed was consistently greater than 30 m s^{-1} for altitudes above about 250 m a.s.l. At the lowest level of flight, the wind speed was greater than 25 m s^{-1}. Using a log scaling law to translate this to surface conditions, the ten meter winds would have been in the range of 17 to 20 m s^{-1}. Gale force winds speed ($\geq$ 17 m s^{-1}) occur regularly over the SO; weather station data from Macquarie Island, which is nearby in the storm track region, had half hourly average surface wind speeds greater than this on about 15 % of days between 2008 and 2011.

3.2 Microphysics variables

Profiles of CDP cloud droplet number concentration and mean diameter, as well as UHSAS aerosol number concentration and 2DC-derived rain rate, calculated from the 2DC observations using droplet fall speeds from Pruppacher et al. (1998), are provided in Fig. 5. Where ρ_L did not meet the criteria discussed in Sect. 2, data from the CDP and UHSAS are shown with dashed lines. More information about particle size within cloud and below cloud base is given by the particle size distributions (PSDs) in Fig. 6.

The cloud droplet number concentration N_C in profile 1 was relatively uniform throughout the cloud with a mean value of 45 cm^{-3}, which is perfectly consistent with the established literature (e.g. Boers and Krummel, 1998; Boers et al., 1998; Yum and Hudson, 2004, etc.) on wintertime cloud microphysical conditions over the pristine SO. Cloud droplet mean diameter $\overline{D_C}$ increased from about 10 µm near cloud base to about 27 µm near cloud top. The cloud droplet effective radius (r_e; Hansen and Travis, 1974), calculated from the PSD was 14.4 µm. This is just above the threshold suggested by Rosenfeld and Gutman (1994) for precipitation, and indeed instantaneous rain rates near cloud base of up to 0.2 mm h^{-1} were calculated, with drizzle drops of diameter up to 400 µm observed.

ACPD
15, 25503–25545, 2015

The picture was similar for profile 2, where peak ρ_L values were comparable, but the mean droplet number concentration was higher (N_C = 77 cm^{-3}) and the diameters smaller ($\overline{D_C}$ = 23 µm and r_e = 13 µm near cloud top). The 2DC-derived rain rate for this cloud was much lower, with maximum values around 0.05 mm h^{-1}.

In profile 3, the HIAPER encountered some broken cloud at 900–1000 m a.s.l., and contiguous cloud between 167 m a.s.l. (the minimum altitude reached) and 700 m a.s.l. In the deeper cloud ρ_L was quite variable, but N_C was uniformly about 100 cm^{-3} in the top 300 m, and increased to about 150 cm^{-3} between 167 and 400 m a.s.l., with peak values above 200 cm^{-3}. $\overline{D_C}$ tended to vary with ρ_L, and had a average value of 14 µm, and r_e near cloud top was about 8.6 µm. Virtually no drops larger than 100 µm were imaged by the 2DC.

In profile 4 the HIAPER appears to have flown through patchy or broken cloud, with ρ_L falling below both the 0.05 and the 0.01 gm^{-3} thresholds at several points during the profile. Within the patchy cloud it is difficult to establish a representative N_C value, because over any given averaging interval there may have been a mixture of clear air and cloud. In a ten-second interval near cloud top, the mean value was 144 cm^{-3}, but where $\rho_L \geq 0.05$ gm^{-3} the mean value was 188 cm^{-3}. The 1 Hz peak values, which are possibly the best estimate of the "adiabatic" cloud droplet concentration (Yum and Hudson, 2004), were up to 300 cm^{-3}. $\overline{D_C}$ varied very little from 10–12 µm, and r_e near cloud top was 7.0 µm. Very few drizzle drops greater than 100 µm diameter were observed in this profile.

UHSAS aerosol concentration (N_U; fourth panel of Fig. 5) observations are not a direct measurement of cloud condensation nuclei (CCN) concentrations, but they are all that was available for sub-micron airborne particles during HIPPO-4. One of the first things that we noted was the particularly low concentration of particles immediately above the boundary layer in each of the four profiles. Values of $N_U \sim$ 10–20 cm^{-3} were typical (except for profile 2, see Sect. 4.1). To put these values in context, at similar latitudes in HIPPO-4 RF10, a flight from Midway to Anchorage, Alaska on 7 July 2011,

ACPD
15, 25503–25545, 2015

tropospheric N_U values (not shown) were typically above 100 cm^{-3} and values above 500 cm^{-3} were observed in two profiles.

In profile 1, there is a large spike in N_U at cloud top, with values reaching well above 600 cm^{-3}, which is likely an artifact of splashing droplets. We discuss this further in Sect. 5.2. In clear air below the cloud, N_U of 74 cm^{-3} (which corresponded to 1.6 times N_C), were observed. The median diameter of the observed particles was 0.143 µm.

Profile 2 shows a similar but smaller spike in N_U at cloud top which we again attribute to droplet breakup. Below-cloud values were on average 113 cm^{-3}, or about 1.5 times N_C, with a broader accumulation mode, with median diameter of 0.174 µm. Just above cloud, at about 1500 m a.s.l., N_U reached 100 cm^{-3} in a layer about 300 m deep; an interesting feature which we discuss in Sect. 4.2.

The HIAPER did not descend below cloud base during profile 3, so a size distribution is not shown for this profile. However, relatively clear air between clouds at 700 and 850 m a.s.l. was sampled. In this gap N_U was about 150 cm^{-3}, but this might not be representative of below-cloud values.

The average value of N_U in the lowest leg of profile 4 was 383 cm^{-3} below cloud base. This is more then double the mean N_C value, but as discussed above, in-cloud N_C might be better represented by values of 200–300 cm^{-3}, which would mean that $N_U \simeq 1.5 N_C$. The size of these aerosol particles was similar to that in profiles 1 and 2, with median diameter 0.143 µm.

3.3 Summary of flight data observations

During a single flight the HIAPER sampled boundary layer cloud, all at temperatures above 0 °C, in a range of different meteorological conditions. In the northernmost profiles (1 and 2), the boundary layer structure was "typical" for the SO: fairly well-mixed (in particular for profile 1) and neutrally stable, and capped with stratocumulus cloud. The microphysical conditions were within the envelope of expected values for the SO. To the south, conditions were much more stable (although still conditionally unstable)

ACPD
15, 25503–25545, 2015

and poorly-mixed, and were characterized by high shear in gale-force winds. The values of N_C and N_U were well outside the envelope that we would expect for pristine maritime conditions over the SO based on previous in-situ studies. In both the northern and southern profiles, N_C in cloud and N_U below cloud were related by a factor of about 1.5.

4 Airmass identification

In this section we present an analysis of back trajectories calculated as per Sect. 2.4, at points along the flight path of the HIAPER during HIPPO-4 RF06, to provide further context for our assessment of the microphysical and atmospheric chemistry observations below.

4.1 Back trajectories

Figure 7 shows ensembles of back trajectories for profiles 1 and 2. For profile 1, the most "classic" of the profiles, the westerly motion two to three days before arriving along the flight track occurred while the subtropical ridge was confined to the continent some 48 h earlier (not shown), resulting in strong westerly winds along 40° S. As the blocking anticyclone moved and intensified over Tasmania, the trajectories stagnated and turned southwards with the approach of the cold front. The vertical motion was weakly descending and there was very little spread between the trajectories, as expected in the weak subsidence beneath the anticyclone. None of the ensemble members appear to pass over the mainland, but some cross over the coastline of remote western Tasmania.

In profile 2, it is evident from the spacing of the 3 hourly markers in the "deterministic" trajectories that the winds were much stronger than for profile 1. Although far displaced from the cold front itself, these trajectories were more clearly driven by the pre-frontal motion, which is shown especially by the gradual ascent (about 1.5 cm s^{-1})

ACPD
15, 25503–25545, 2015

in the 3000 m ensemble during the 20 h prior to arrival, and in the 1500 m ensemble during the 10 h prior to arrival. All of the ensembles include trajectories which appear to have spent time over the coastal mainland immediately before strong advection from the north. The 1500 m a.s.l. "deterministic" trajectory and a large number of the ensemble members passed in the general vicinity of Port Pirie, a heavy industry center in South Australia, some 24 to 36 h before arriving at the location of profile 2. The same was true for an ensemble arriving at 3000 m, but this is not shown. None of the members for the 4500 m ensemble passed over land.

The trajectories for profile 3 (Fig. 8) are considerably more complex. Our estimate for the distance ahead of the cold front, accounting for frontal motion between the ERA-Interim analysis at 00:00 UTC (Fig. 1) and the time on location, is about 200 km. It appears that some of the trajectory ensemble members were initialized to the west of (i.e. behind) the cold front, and others to the east, because there was considerable divergence in the airmass history. For each arrival height, some of the ensemble members originated from around the Nullarbor Plain, an unpopulated and sparsely vegetated coastal region in Western and South Australia; and some members originated over the remote Indian/Southern Ocean and did not pass over any land. The bifurcation is apparent in the trajectory altitude as well: those that originated near the continent (around 130° E, 30° S) ahead of the front generally had ascending trajectories in the 20 h prior to arrival at profile 3, and those that originated over the remote oceans had descending trajectories.

Profile 4 was performed even closer to the cold front, so there is again substantial divergence in the airmass history. Based on the location provided in the ERA-Interim analysis, the aircraft was about 160 km ahead of the cold front, but the "deterministic" trajectories appear to have been initialized behind the front in the GDAS analysis. Although none of the ensemble members arriving at either 500 or 1500 m a.s.l. passed over directly land, a group arriving at 500 m a.s.l. originated from near the South Australian coastline some 48 h earlier. On the other hand, the group of trajectories with

ACPD
15, 25503–25545, 2015

pre-frontal characteristics arriving at 4000 m a.s.l. were over south Western Australia at low altitudes about 24 h earlier.

In summary, the profile with the strongest case for continental/anthropogenic influence is profile 2, which had ensemble members at all levels passing nearby known areas of industrial activity. The likelihood of interaction with continental/anthropogenic aerosol sources decreased for profiles further to the south, where there was some evidence for continental contribution at around 4000 m a.s.l., but not within the boundary layer.

4.2 Analysis of chemistry data with respect to back trajectories

Figure 9 shows CO, BC, and N_U for the entire vertical extent of the four profiles. In profile 1, there was a weak increase in CO (up to 60 ppbv) and N_U (up to 75 cm^{-3}) between 2000 and 4000 m, but no signal in BC and minimal interaction with the continental airmass. CO also increased with height above 5500 m, but there was no signal in either BC or N_U at these levels. The air in profile 1 could be described as very clean, with no clear indication of continental influence.

The strongest chemical signal in profile 2, and indeed all of the profiles, is in a layer between 4000 and 5000 m a.s.l., where elevated, highly correlated CO and BC concentrations were observed. This is characteristic of combustion, but we found that trajectories arriving at 4500 m a.s.l. did not have the clear terrestrial interaction that 1500 and 3000 m (not shown) a.s.l. trajectories had, and aerosol concentrations were quite low ($N_U \simeq 30\,cm^{-3}$) at these levels. Just above cloud top at 1500 m a.s.l., N_U was slightly elevated at 100 cm^{-3}, which corresponded to a small increase in both CO and BC, and the back trajectories at this level had a clear terrestrial interaction. In any case, if these observations are indeed evidence of long range transport of anthropogenic pollution, the impact on the aerosol loading was small.

If there was terrestrial interaction for the air sample in profile 3, the signals in the observations were weak. BC observations were unfortunately missing at 3000–

ACPD
15, 25503–25545, 2015

4000 m a.s.l., but slightly elevated CO concentrations at about 4000 m a.s.l. correspond to increased N_U of about 50 cm^{-3} from values of 10–20 cm^{-3} just above the boundary layer.

At 4000 m a.s.l. in profile 4, there was a slight increase in the tropospheric CO concentration, with values up to 60 ppbv, or 10 ppbv higher than the values at the top of the boundary layer. This corresponded to a small peak in the N_U concentration of about 80 cm^{-3}, but BC observations, which were trending upwards with altitude below this, were missing here as well. Given that some of the trajectory ensemble members originated over land at low altitude, this could be evidence of diluted continental or anthropogenic influence. This feature is clearly decoupled from the boundary layer, as evidenced by N_U values strictly below 20 cm^{-3} between 1250 and 2000 m a.s.l. Within the boundary layer itself, CO concentrations decrease with height from 54 ppbv at 167 m a.s.l. to 50 ppbv at 1250 m a.s.l. This negative CO gradient could be argued to correspond to the group of trajectories that passed near land, but a marine source below a poorly-mixed boundary layer could also account for this. In any case, N_U varied much more in the boundary layer than it did near 4000 m a.s.l. for a similar variation in CO.

4.3 Comparison to clearly polluted/pristine cases

It is useful to provide some context to our discussion of a possible anthropogenic pollution plume by considering some other flights. In HIPPO-4 RF07 (the subsequent flight, two days later), the HIAPER flew from Hobart to Darwin and performed a descending and an ascending profile over the Bass Straight, almost directly south of Melbourne. Conditions (not shown) were somewhat different to profile 1 of RF06, with a deeper boundary layer (capping inversion at 1900 m a.s.l.); lower wind speed (about 10 m s^{-1}); and there was no cloud. The wind direction between 600 and 1500 m a.s.l. was directly from the north, and in this layer the pollution plume from the Melbourne urban area can be unequivocally identified in Fig. 10, which shows observations for the entire vertical extent of the profiles of θ, CO, BC, and N_U. Concentrations of CO were

ACPD
15, 25503–25545, 2015

about 20–30 ppmv higher within the plume than in the free troposphere. N_U of up to 2000 cm^{-3} was observed, and the values were very highly correlated with both BC and CO concentrations (R = 0.87 and R = 0.95 respectively).

In HIPPO-3 RF06 (not shown), a return flight from Christchurch to 67° S in the previous campaign (April 2010) and the subject of Chubb et al. (2013), undoubtedly pristine maritime conditions were encountered. Low-level CO concentrations were about 41 ppbv (this may be a seasonal difference compared to HIPPO-4 RF06), but still varied by about 5 ppbv between 5000 and 7000 m a.s.l. BC concentrations were practically zero in all profiles, and N_U concentrations were less than 20 cm^{-3} in the free troposphere but rose to around 100 cm^{-3} in the lowest levels sampled.

With these two comparison flights in mind, HIPPO-4 RF06 (the present flight) is neither an example of a pristine SO environment nor a heavily modified one. As discussed above, there is mixed evidence for anthropogenic influence in each of the profiles. However, the weak signals that can be identified occur well above the boundary layer, where back trajectories can in some cases be used link the history of the air to anthropogenic sources. The air within the boundary layer, on the other hand, does not display an anthropogenic signature that could explain the elevated N_U values.

4.4 What about mineral dust?

So far our analysis has concentrated on sources of aerosol associated with combustion, and therefore associated with CO and BC. However, there is the possibility that naturally occurring continental dust could have been the cause of the elevated N_U and N_C values in profiles 3 and 4. Indeed, dust from the Australian continent has been hypothesized to be an important fertilizing agent for SO phytoplankton (Martin, 1990), and dust samples from Antarctica have been geochemically linked to Australian sources (Revel-Rolland et al., 2006).

While the principal sources of Australian dust are further to the east in the Murray–Darling Basin (De Deckker et al., 2010), the Nullarbor Plain is a known secondary

ACPD
15, 25503–25545, 2015

source of dust. However, the month of June 2011 was relatively wet in the Nullarbor Plain, temperatures were about average for winter, and wind speeds in the days before HIPPO-4 RF06 were unremarkable. Furthermore, observations of suspended dust are routinely reported at Australian Bureau of Meteorology from a number of sites in the Nullarbor (O'Loingsigh et al., 2014), and there were no reports of any suspended dust in the week before the flight (T. O'Loingsigh, personal communication, 2015).

Another argument comes directly from the trajectories (and as such applies also to the hypothesis of anthropogenic aerosols): the trajectories with continental interaction arriving at 500 and 1500 m a.s.l. in profile 3 are very similar, both in the horizontal and vertical. If the elevated N_U values in the boundary layer were due to dust, we should expect to find similar N_U values at 1500 m as well, but they were an order of magnitude lower. The same argument applies to profile 4, where trajectories arriving at 4000 m a.s.l. may have been near the surface of south Western Australia about 36 h before, but N_U values at these levels were small in comparison to the boundary layer values.

4.5 Can we explain elevated droplet and aerosol concentrations by considering potential anthropogenic or continental sources?

To summarize the results of this section, we used the combination of back trajectory ensembles with in-situ observations as a tool to identify continental/anthropogenic aerosol influences. In profiles 3 and 4 there was evidence of weak anthropogenic influence between 3000 and 5000 m a.s.l. through the increase of N_U in association with BC and CO. When compared to profiles through a clear pollution plume in another flight, it is evident that any influence in HIPPO-4 RF06 was highly diluted. Furthermore, given similar CO signals in the boundary layer as in the upper levels, the N_U values were far too high to be attributed to anthropogenic pollution. In addition, we were unable to identify any dust storm activity around the Nullarbor in the week before the flight, and surface observations suggest that dust activity was unlikely. The trajectory analysis suggested that dust, if present, should have resulted in similarly increased N_U values

ACPD
15, 25503–25545, 2015

in both the troposphere and the boundary layer, but there was an order of magnitude difference between the two.

The conclusion that we draw from this analysis is that the elevated N_C and N_U values within the boundary layer can not be predominantly attributed to long-range transport of anthropogenic pollution or continental dust.

5 Evaluation of uncertainties

5.1 CDP observations

The accuracy of the CDP is typically stated as ±10 % due to uncertainties in the true sample volume and in the sizing of small particles through Mie scattering. Using an parcel ascent model (which conserved θ_e) initialized with conditions near cloud base for profile 1, we calculated the theoretical adiabatic ρ_L for this cloud. This calculation suggested that the value at cloud top would be about 0.64 gm^{-3}, very close to the observed value of 0.60 gm^{-3}. When all observations within this cloud were compared to the theoretical adiabatic values through linear regression, excluding a small region where entrained air was apparent, the observations were found to agree to within 1 %. This suggests very strongly that the CDP observations were robust.

5.2 UHSAS observations in ambiguous conditions

Vidaurre and Hallett (2009) established droplet breakup criteria upon impact with a cylindrical surface based on the Weber number, or the ratio of particle impact kinetic energy to surface energy. This depended primarily on particle diameter and speed of impact (which is in turn dependent on the inlet geometry). For a representative airspeed of the HIAPER and geometry of the UHSAS inlet, their criteria predict that droplet breakup should be minimal for droplets with diameters under about 8 µm, but severe for droplets with diameters over about 20 µm.

ACPD
15, 25503–25545, 2015

In profiles 1 and 2, the air beneath the cloud was unequivocally clear, with zero N_C observed by the CDP, so we have no concerns about droplet splashing affecting these data.

In profile 3, the cloud-free $\rho_L < 0.01\,\mathrm{gm}^{-3}$ threshold was never met in the lowest leg and droplet diameters of 10–12 µm were observed. These droplet sizes could have caused splashing on the UHSAS inlet so we do not consider these data. However there was some suitably clear air for a short interval between clouds during descent, and we consider these data to be usable, although perhaps not representative of below-cloud values.

The case for the robustness of the UHSAS data in profile 4 is much better. The air sampled at the lowest leg met our "probably clear" criterion of $\rho_L < 0.05\,\mathrm{gm}^{-3}$. However, there was a non-zero cloud droplet concentration in most one-second intervals, and N_C was in the range of 6–10 cm^{-3} (ρ_L was 0.001–0.005 gm^{-3}), with particles of mean diameter 6–7 µm. We interpret these conditions as hazy sub-cloud air, and according to the work of Vidaurre and Hallett (2009), we expect that droplet splashing should not affect the observations. Indeed, setting the "probably clear" ρ_L threshold as low as $0.002\,\mathrm{gm}^{-3}$ revealed very little sensitivity in N_C. We are thus highly confident that the average values of $N_U \simeq 383\,\mathrm{cm}^{-3}$ below cloud base were indeed reliable for profile 4.

5.3 Uncertainties in back trajectories

In general, the accuracy of back trajectories depends on the accuracy of the wind fields in the gridded data, but is also influenced by temporal and spatial resolution of the product used (Rolph and Draxler, 1990). For trajectories over the open ocean, the 3 hourly one degree dataset used is sufficient to resolve the synoptic scale features which are dominant, at least in the free troposphere.

The way that vertical motion is handled can be important: horizontal wind components generally vary with height, so any vertical displacement errors will contribute to horizontal displacement errors as well. Vertical winds are generally deduced from the

ACPD
15, 25503–25545, 2015

divergence of the horizontal components and can be noisy. It is possible to calculate isentropic trajectories, which follow surfaces of constant θ, which is a good approximation to the motion of dry air in the free troposphere. However, this assumption is not useful in the boundary layer where θ is well-mixed, or in regions where vertical motion due to moist convection may be present, so using modeled vertical velocities was a better choice.

We are interested in boundary layer conditions for the purposes of this paper, but acknowledge that boundary layer trajectories are especially prone to the uncertainties mentioned above, especially in highly sheared environments. In addition, the representation of boundary layer structure over the SO in global reanalyses is known to be questionable (e.g. Hande et al., 2012b; Huang et al., 2015). We chose to analyze trajectories arriving at multiple levels, with two of the three ensembles for each profile initialized above the boundary layer, with this concern in mind.

The task of simulating back trajectories for HIPPO-4 RF06 presents an additional challenge in that the region is experiencing a rapid dynamical change in the form of an approaching cold front. The heterogeneity of the wind field in this situation compounds the uncertainties in the back trajectory due to inaccuracies in the meteorological analysis. We used an ensemble approach to represent the uncertainty in the airmass history. For profiles 1 and 2, the location was sufficiently far from the cold front that the wind field heterogeneity did not overly influence the back trajectories. There was still some variability amongst the ensemble members, but the "deterministic" trajectories should be accurate. For profiles 3 and 4, the perturbation in the initialization points was sufficient to straddle the cold front, resulting in two "clusters" of trajectories for each ensemble. The spread in each of these clusters was comparable to the spread of the entire ensembles for profiles 1 and 2. The in-situ observations suggest that the profiles were performed ahead of the cold front, which suggests that the more northerly clusters were the most representative.

ACPD
15, 25503–25545, 2015

6 Discussion and conclusions

6.1 Summary of arguments presented in this paper

Downey et al. (1990) argued that long range transport of aerosol from the Australian continent was responsible for cases of high CN concentrations at Macquarie Island, but it seems that a direct hit on an urban center was required, and they reported high correlation with radon (a continental tracer) in these instances. We used CO and BC as continental/anthropogenic markers, and showed that they were very effective in identifying the pollution plume from Melbourne in HIPPO-4 RF07.

Of the four vertical profiles performed in HIPPO-4 RF06, the one with the most convincing signature of anthropogenic/continental influence was profile 2, where a clear correlation between CO and BC was observed, possibly in several layers. The strongest signature was found between 4000 and 5000 m a.s.l., but even here there was no correlation to the sub-micron particle number concentration N_U. Better correlation between the three values was identified at 1500 m a.s.l., where peak N_U values were over 100 cm^{-3}, and back trajectories clearly suggest a terrestrial pollution source. In the boundary layer clouds sampled in profile 2, mean cloud droplet number concentrations were about 77 cm^{-3}, which is not particularly unusual for the remote SO.

For profiles 3 and 4 we have argued that the most likely signature of anthropogenic/continental influence was well above and decoupled from the boundary layer, and that N_U at those levels was insignificant in comparison to values within the boundary layer. The trajectories that arrived in the boundary layer for profiles 3 and 4 show much weaker evidence for anthropogenic/continental influence, and were not coincidental with a trajectory from any industrial/urban centers. Yet the N_C and N_U values in profile 4 were about twice those of profile 2, and up to four times the values for profile 1. The very small increase in CO in the boundary layer may suggest a highly diluted anthropogenic signature, but it is not nearly of sufficient magnitude to explain the N_U values. The microphysical results for profile 3 were similar, but we have somewhat

ACPD
15, 25503–25545, 2015

less confidence in the UHSAS concentrations due to the potential for artifacts due to splashing droplets.

While N_C values of 150–300 cm^{-3} are by no means exceptional in a global context, they are unexpected for the pristine maritime environment of the SO, especially during wintertime when ocean productivity is lowest. If the hypothesis that such values were predominantly caused by long range transport of continental pollutants can be rejected, as we argue in this paper, then we are left with the conclusion that the elevated particle concentration observed by the UHSAS, which probably includes most of the CCN, was produced locally. We consider sea spray aerosol to be the best candidate to explain the elevated aerosol concentrations, and indeed there are many studies that suggest that SSA can dominate the marine boundary layer CCN population (e.g. Clarke et al., 2006; Murphy et al., 1998).

6.2 General discussion of results

Our conclusions contrast with the findings of Blot et al. (2013), which suggest that wind speed was not a factor in controlling SSA concentrations in the VOCALS campaign, and other authors (Bates et al., 1998; Covert et al., 1998; Berg et al., 1998) have also reported poor correlations of SSA concentrations with wind speed. However, the low level wind speeds of 25–35 m s^{-1} encountered during profiles 3 and 4 was extreme, and well outside the ranges reported by Blot et al. (2013). Because the background aerosol concentrations were so low in this region, the additional SSA production would have had a significant impact on overall CCN as well as N_C.

This result is of interest in discussions of the cloud structure and radiation bias over the SO. Strong boundary layer winds, such as those encountered in HIPPO-4 RF06, are a regular occurrence over the SO. Moreover, Korhonen et al. (2010) showed an increase in wind speed in the latitude band 50–65° S from 1980 to 2002 in reanalysis data, which has been verified observationally by Hande et al. (2012a). Over the same period, modeled CCN concentrations increased by 19 % on average, and they found that wind speed accounted for 48 % of the variance and was the most important cause

ACPD
15, 25503–25545, 2015

of the changes. The resultant negative radiative forcing in this latitudinal band was on the same order as the positive forcing due to greenhouse gases.

The CCN concentrations for the study of Korhonen et al. (2010) were derived from a global aerosol model which includes a wind speed dependent SSA parameterization, but the basis for such parameterizations has been questioned by several authors, as discussed in this paper. Nevertheless, the hypothesis that SSA could be a factor in such a climate feedback mechanism is supported by the observations of HIPPO-4 RF06. Targeted observations are clearly needed to more convincingly address this hypothesis, which fits squarely within the stated priorities of the NSF Advisory Committee for Geosciences (2014).

7 Conclusions

In this paper, we have presented thermodynamic, microphysical and atmospheric chemistry observations from vertical profiles performed during HIPPO-4 RF06. Large variation in microphysical characteristics of the boundary layer clouds and the aerosol concentration were found, and in particular the CDP cloud droplet number concentration N_C and UHSAS aerosol concentration N_U were substantially higher (by a factor of two to five) than expected for the southernmost profiles. At these latitudes the wind speeds were the most extreme, at 25–35 m s^{-1} at very low altitudes (about 167 m a.s.l.). We were unable to attribute these observations to continental/anthropogenic sources through the analysis of the atmospheric chemistry data and back trajectories, although there were indications of weak impacts at much higher altitudes in the profiles. We conclude that local production of sea spray aerosol through the high winds in the southernmost regions of the flight is the most likely explanation for these observations.

Acknowledgements. This research was funded by ARC linkage grant LP120100115 and relies on datasets produced for the HIPPO deployments, and made available to the community by the National Center for Atmospheric Research's Earth Observing Laboratory. The National Center for Atmospheric Research is sponsored by the National Science Foundation.

ACPD
15, 25503–25545, 2015

References

Bates, T. S., Kapustin, V. N., Quinn, P. K., Covert, D. S., Coffman, D. J., Mari, C., Durkee, P. A., De Bruyn, W. J., and Saltzman, E. S.: Processes controlling the distribution of aerosol particles in the lower marine boundary layer during the First Aerosol Characterization Experiment (ACE 1), J. Geophys. Res.-Atmos., 103, 16369–16383, 1998. 25507, 25528

Bennartz, R.: Global assessment of marine boundary layer cloud droplet number concentration from satellite, J. Geophys. Res.-Atmos., 112, D02201, doi:10.1029/2006JD007547, 2007. 25506

Berg, O. H., Swietlicki, E., and Krejci, R.: Hygroscopic growth of aerosol particles in the marine boundary layer over the Pacific and Southern Oceans during the First Aerosol Characterization Experiment (ACE 1), J. Geophys. Res.-Atmos., 103, 16535–16545, 1998. 25507, 25528

Blot, R., Clarke, A. D., Freitag, S., Kapustin, V., Howell, S. G., Jensen, J. B., Shank, L. M., McNaughton, C. S., and Brekhovskikh, V.: Ultrafine sea spray aerosol over the southeastern Pacific: open-ocean contributions to marine boundary layer CCN, Atmos. Chem. Phys., 13, 7263–7278, doi:10.5194/acp-13-7263-2013, 2013. 25507, 25528

Boers, R. and Krummel, P. B.: Microphysical properties of boundary layer clouds over the Southern Ocean during ACE 1, J. Geophys. Res.-Atmos., 103, 16651–16663, 1998. 25505, 25515

Boers, R., Jensen, J., Krummel, P., and Gerber, H.: Microphysical and short-wave radiative structure of wintertime stratocumulus clouds over the Southern Ocean, Q. J. Roy. Meteor. Soc., 122, 1307–1339, 1996. 25505

Boers, R., Jensen, J., and Krummel, P.: Microphysical and short-wave radiative structure of stratocumulus clouds over the Southern Ocean: summer results and seasonal differences, Q. J. Roy. Meteor. Soc., 124, 151–168, 1998. 25505, 25515

Boutle, I. A., Abel, S. J., Hill, P. G., and Morcrette, C. J.: Spatial variability of liquid cloud and rain: observations and microphysical effects, Q. J. Roy. Meteor. Soc., 140, 583–594, doi:10.1002/qj.2140, 2014. 25511

Cai, Y., Montague, D. C., Mooiweer-Bryan, W., and Deshler, T.: Performance characteristics of the ultra high sensitivity aerosol spectrometer for particles between 55 and 800 nm: laboratory and field studies, J. Aerosol Sci., 39, 759–769, 2008. 25510

ACPD
15, 25503–25545, 2015

Charlson, R. J., Lovelock, J. E., Andreae, M. O., and Warren, S. G.: Oceanic phytoplankton, atmospheric sulphur, cloud albedo and climate, Nature, 326, 655–661, 1987. 25505
Chubb, T. H., Jensen, J. B., Siems, S. T., and Manton, M. J.: In situ observations of supercooled liquid clouds over the Southern Ocean during the HIAPER Pole-to-Pole Observation campaigns, Geophys. Res. Lett., 40, 5280–5285, 2013. 25506, 25522
Clarke, A. D., Owens, S. R., and Zhou, J.: An ultrafine sea-salt flux from breaking waves: implications for cloud condensation nuclei in the remote marine atmosphere, J. Geophys. Res.-Atmos., 111, D06202, doi:10.1029/2005JD006565, 2006. 25528
Covert, D. S., Gras, J. L., Wiedensohler, A., and Stratmann, F.: Comparison of directly measured CCN with CCN modeled from the number-size distribution in the marine boundary layer during ACE 1 at Cape Grim, Tasmania, J. Geophys. Res.-Atmos., 103, 16597–16608, 1998. 25507, 25528
Day, J.: Production of droplets and salt nuclei by the bursting of air-bubble films, Q. J. Roy. Meteor. Soc., 90, 72–78, 1964. 25506
De Deckker, P., Norman, M., Goodwin, I. D., Wain, A., and Gingele, F. X.: Lead isotopic evidence for an Australian source of aeolian dust to Antarctica at times over the last 170,000 years, Palaeogeography, Palaeoclimatology, Palaeoecology, 285, 205–223, doi:10.1016/j.palaeo.2009.11.013, 2010. 25522
de Leeuw, G., Andreas, E. L., Anguelova, M. D., Fairall, C., Lewis, E. R., O'Dowd, C., Schulz, M., and Schwartz, S. E.: Production flux of sea spray aerosol, Rev. Geophys., 49, RG2001, doi:10.1029/2010RG000349, 2011. 25507
Downey, A., Jasper, J., Gras, J., and Whittlestone, S.: Lower tropospheric transport over the Southern Ocean, J. Atmos. Chem., 11, 43–68, 1990. 25507, 25527
Draxler, R. and Hess, G.: An overview of the HYSPLIT_4 modelling system for trajectories, dispersion and deposition, Aust. Meteorol. Mag., 47, 295–308, 1998. 25512
Gerbig, C., Schmitgen, S., Kley, D., Volz-Thomas, A., Dewey, K., and Haaks, D.: An improved fast-response vacuum-UV resonance fluorescence CO instrument, J. Geophys. Res.-Atmos., 104, 1699–1704, 1999. 25511
Grosvenor, D. P. and Wood, R.: The effect of solar zenith angle on MODIS cloud optical and microphysical retrievals within marine liquid water clouds, Atmos. Chem. Phys., 14, 7291–7321, doi:10.5194/acp-14-7291-2014, 2014. 25506
Hande, L., Siems, S., and Manton, M.: Observed trends in wind speed over the Southern Ocean, Geophys. Res. Lett., 39, L11802, doi:10.1029/2012GL051734, 2012a. 25528

ACPD
15, 25503–25545, 2015

Hande, L., Siems, S., Manton, M., and Belusic, D.: Observations of wind shear over the Southern Ocean, J. Geophys. Res.-Atmos., 117, doi:10.1029/2012JD017488, 2012b. 25514, 25526

Hansen, J. E. and Travis, L. D.: Light scattering in planetary atmospheres, Space Sci. Rev., 16, 527–610, 1974. 25515

Huang, Y., Franklin, C. N., Siems, S. T., Manton, M. J., Chubb, T., Lock, A., Alexander, S., and Klekociuk, A.: Evaluation of boundary-layer cloud forecasts over the Southern Ocean in a limited-area numerical weather prediction system using in situ, space-borne and ground-based observations, Q. J. Roy. Meteor. Soc., 141, 2259–2276, doi:10.1002/qj.2519, 2015. 25526

Korhonen, H., Carslaw, K. S., Forster, P. M., Mikkonen, S., Gordon, N. D., and Kokkola, H.: Aerosol climate feedback due to decadal increases in Southern Hemisphere wind speeds, Geophys. Res. Lett., 37, L02805, doi:10.1029/2009GL041320, 2010. 25528, 25529

Lance, S., Brock, C. A., Rogers, D., and Gordon, J. A.: Water droplet calibration of the Cloud Droplet Probe (CDP) and in-flight performance in liquid, ice and mixed-phase clouds during ARCPAC, Atmos. Meas. Tech., 3, 1683–1706, doi:10.5194/amt-3-1683-2010, 2010. 25510

Lewis, E. R. and Schwartz, S. E.: Sea salt aerosol production: mechanisms, methods, measurements, and models – a critical review, EOS T. Am. Geophys. Union, doi:10.1002/9781118666050, 2004. 25506, 25507

Marks, R.: Preliminary investigations on the influence of rain on the production, concentration, and vertical distribution of sea salt aerosol, J. Geophys. Res.-Oceans, 95, 22299–22304, 1990. 25507

Martin, J. H.: Glacial-interglacial CO_2 change: the Iron Hypothesis, Paleoceanography, 5, 1–13, 1990. 25522

Meehl, G. A., Covey, C., Taylor, K. E., Delworth, T., Stouffer, R. J., Latif, M., McAvaney, B., and Mitchell, J. F.: The WCRP CMIP3 multimodel dataset: a new era in climate change research, B. Am. Meteorol. Soc., 88, 1383–1394, 2007. 25504

Murphy, D. M., Anderson, J. R., Quinn, P. K., McInnes, L. M., Brechtel, F. J., Kreidenweis, S. M., Middlebrook, A. M., Pósfai, M., Thomson, D. S., and Buseck, P. R.: Influence of sea-salt on aerosol radiative properties in the Southern Ocean marine boundary layer, Nature, 392, 62–65, doi:10.1038/32138, 1998. 25528

ACPD
15, 25503–25545, 2015

Nakajima, T. and King, M. D.: Determination of the optical thickness and effective particle radius of clouds from reflected solar radiation measurements. Part I: Theory, J. Atmos. Sci., 47, 1878–1893, 1990. 25506

Nilsson, E., Rannik, Ü., Swietlicki, E., Leck, C., Aalto, P. P., Zhou, J., and Norman, M.: Turbulent aerosol fluxes over the Arctic Ocean: 2. Wind-driven sources from the sea, J. Geophys. Res.-Atmos., 106, 32139–32154, 2001. 25507

NSF Advisory Committee for Geosciences: Dynamic Earth: GEO Imperatives and Frontiers 2015–2020, Tech. rep., National Science Foundation, Arlington, VA 22230, USA, 2014. 25505, 25529

O'Dowd, C. D. and Smith, M. H.: Physicochemical properties of aerosols over the northeast Atlantic: evidence for wind-speed-related submicron sea-salt aerosol production, J. Geophys. Res.-Atmos., 98, 1137–1149, 1993. 25507

O'Loingsigh, T., McTainsh, G., Tews, E., Strong, C., Leys, J., Shinkfield, P., and Tapper, N.: The Dust Storm Index (DSI): a method for monitoring broadscale wind erosion using meteorological records, Aeolian Res., 12, 29–40, 2014. 25523

Pruppacher, H. R., Klett, J. D., and Wang, P. K.: Microphysics of clouds and precipitation, Kluwer Academic Publishers, P.O. Box 17, 3300 AA Dordrecht, the Netherlands, 1998. 25515

Quinn, P. and Bates, T.: The case against climate regulation via oceanic phytoplankton sulphur emissions, Nature, 480, 51–56, 2011. 25505

Revel-Rolland, M., De Deckker, P., Delmonte, B., Hesse, P., Magee, J., Basile-Doelsch, I., Grousset, F., and Bosch, D.: Eastern Australia: a possible source of dust in East Antarctica interglacial ice, Earth Planet. Sc. Lett., 249, 1–13, 2006. 25522

Rolph, G. and Draxler, R.: Sensitivity of three-dimensional trajectories to the spatial and temporal densities of the wind field, J. Appl. Meteorol., 29, 1043–1054, 1990. 25525

Romashkin, P.: NCAR GV (HIAPER) Low Rate (LRT – 1 sps) Navigation, State Parameter, and Microphysics Flight-Level Data, Tech. rep., UCAR/NCAR – Earth Observing Laboratory, Boulder, CO 80307, USA, available at: http://www.eol.ucar.edu/system/files/PM_notes_HIPPO-4_-5.doc, (last access: 31 August 2015), 2012. 25508

Rosenfeld, D. and Gutman, G.: Retrieving microphysical properties near the tops of potential rain clouds by multispectral analysis of AVHRR data, Atmos. Res., 34, 259–283, 1994. 25515

Russell, L. M., Lenschow, D. H., Laursen, K. K., Krummel, P. B., Siems, S. T., Bandy, A. R., Thornton, D. C., and Bates, T. S.: Bidirectional mixing in an ACE 1 marine boundary layer

ACPD
15, 25503–25545, 2015

overlain by a second turbulent layer, J. Geophys. Res.-Atmos., 103, 16411–16432, 1998. 25514
Salomonson, V. V., Barnes, W., Maymon, P. W., Montgomery, H. E., and Ostrow, H.: MODIS: advanced facility instrument for studies of the Earth as a system, IEEE T. Geosci. Remote, 27, 145–153, 1989. 25506
Schwarz, J. P., Gao, R. S., Fahey, D. W., Thomson, D. S., Watts, L. A., Wilson, J. C., Reeves, J. M., Darbeheshti, M., Baumgardner, D. G., Kok, G. L., Chung, S. H., Schulz, M., Hendricks, J., Lauer, A., Kärcher, B., Slowik, J. G., Rosenlof, K. H., Thompson, T. L., Langford, A. O., Loewenstein, M., and Aikin, K. C.: Single-particle measurements of midlatitude black carbon and light-scattering aerosols from the boundary layer to the lower stratosphere, J. Geophys. Res.-Atmos., 111, D16207, doi:10.1029/2006JD007076, 2006. 25511
Trenberth, K. E. and Fasullo, J. T.: Simulation of present-day and twenty-first-century energy budgets of the southern oceans, J. Climate, 23, 440–454, 2010. 25504
Vidaurre, G. and Hallett, J.: Particle impact and breakup in aircraft measurement, J. Atmos. Ocean. Tech., 26, 972–983, 2009. 25524, 25525
Wofsy, S.: HIAPER Pole-to-Pole Observations (HIPPO): fine-grained, global-scale measurements of climatically important atmospheric gases and aerosols, Philos. T. R. Soc. A, 369, 2073–2086, 2011. 25505, 25508
Wofsy, S. C., Daube, B. C., Jimenez, R., Kort, E., Pittman, J. V., Park, S., Commane, R., Xiang, B., Santoni, G., Jacob, D., Fisher, J., Pickett-Heaps, C., Wang, H., Wecht, K., Wang, Q.-Q., Stephens, B. B., Shertz, S., Watt, A. S., Romashkin, P., Campos, T., Haggerty, J., Cooper, W. A., Rogers, D., Beaton, S., Hendershot, R., Elkins, J. W., Fahey, D. W., Gao, R. S., Moore, F., Montzka, S. A., Schwarz, J. P., Perring, A. E., Hurst, D., Miller, B. R., Sweeney, C., Oltmans, S., Nance, D., Hintsa, E., Dutton, G., Watts, L. A., Spackman, J. R., Rosenlof, K. H., Ray, E. A., Hall, B., Zondlo, M. A., Diao, M., Keeling, R., Bent, J., Atlas, E. L., Lueb, R., and Mahoney, M. J.: HIPPO Merged 10-second Meteorology, Atmospheric Chemistry, and Aerosol Data (R_20121129), Tech. rep., Carbon Dioxide Information Analysis Center, Oak Ridge National Laboratory, Oak Ridge, Tennessee, USA, doi:10.3334/CDIAC/hippo_010, 2012. 25508
Wood, R. and Field, P. R.: The distribution of cloud horizontal sizes, J. Climate, 24, 4800–4816, 2011. 25511
Woodcock, A. H.: Salt nuclei in marine air as a function of altitude and wind force, J. Meteorol., 10, 362–371, 1953. 25507

ACPD
15, 25503–25545, 2015

Yum, S. S. and Hudson, J. G.: Wintertime/summertime contrasts of cloud condensation nuclei and cloud microphysics over the Southern Ocean, J. Geophys. Res.-Atmos., 109, D06204, doi:10.1029/2003JD003864, 2004. 25515, 25516

ACPD
15, 25503–25545, 2015

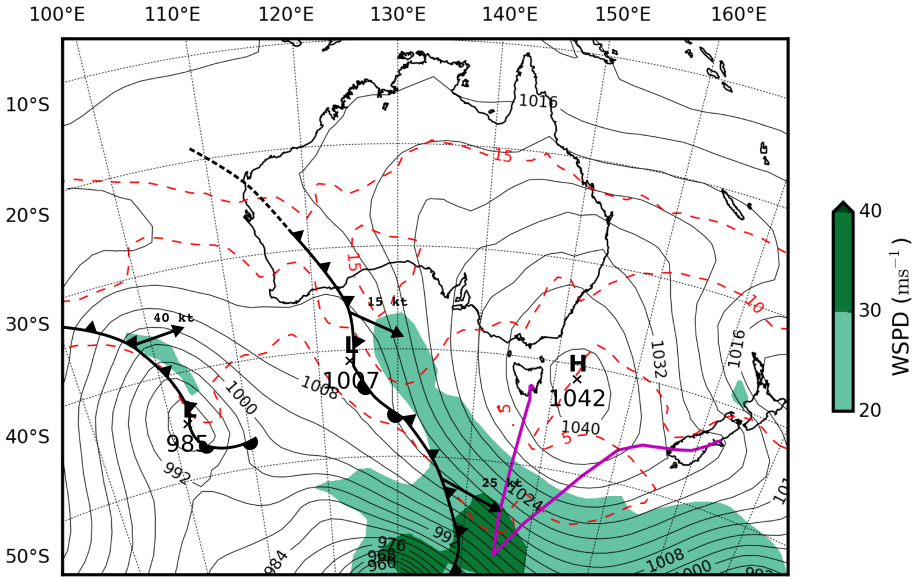

Figure 1. ERA-Interim mean sea level pressure at 00:00 UTC on 29 June 2011, with synoptic features as analyzed by the Australian Bureau of Meteorology, 950 hPa wind speed (colors; m s^{-1}), and 950 hPa temperatures (dashed red contours at 5, 10 and 15 °C). The flight track for HIPPO-4 RF06 is shown in magenta.

ACPD
15, 25503–25545, 2015

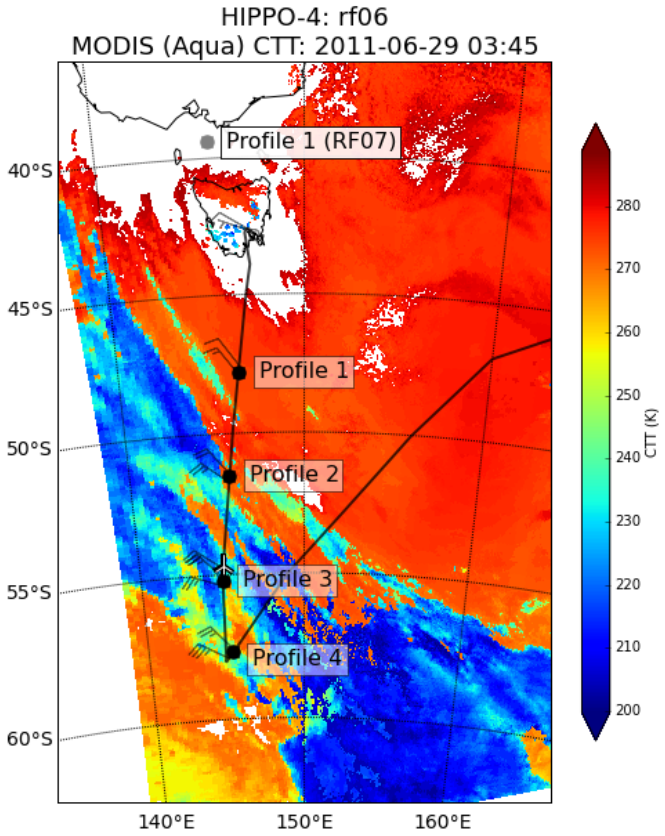

Figure 2. Flight track for HIPPO-4 RF06, with MODIS cloud top temperature overlay. The locations of the lowest level of the four profiles are labeled as per the text.

ACPD
15, 25503–25545, 2015

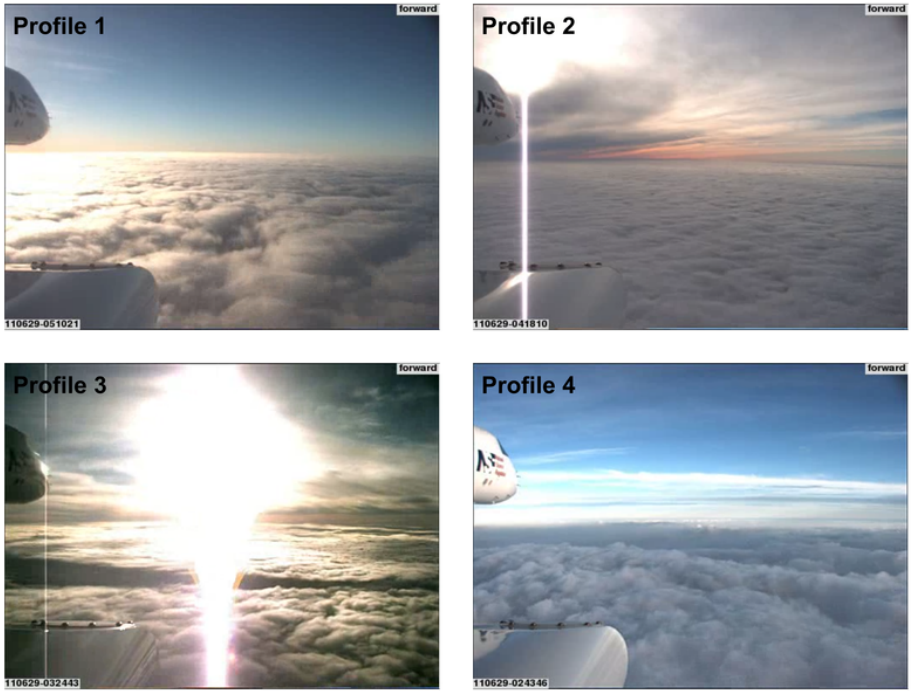

Figure 3. Forward camera imagery of boundary layer cloud top conditions for the four profiles as labeled.

ACPD
15, 25503–25545, 2015

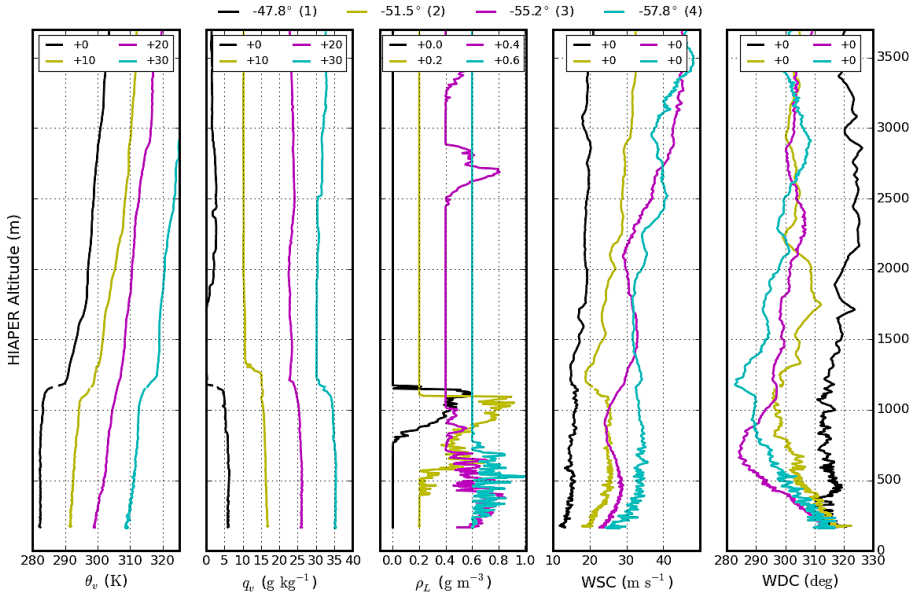

Figure 4. Profiles of thermodynamic variables within and above the boundary layer for RF06. From left: virtual potential temperature (θ_v); specific humidity (q_v); CDP liquid water content (ρ_L); wind speed (WSC); and wind direction (WDC). The colors indicate the profile number and location (see top panel). Note that for display purposes, the values for some profiles have been offset by the amount indicated in the legend in each panel.

ACPD
15, 25503–25545, 2015

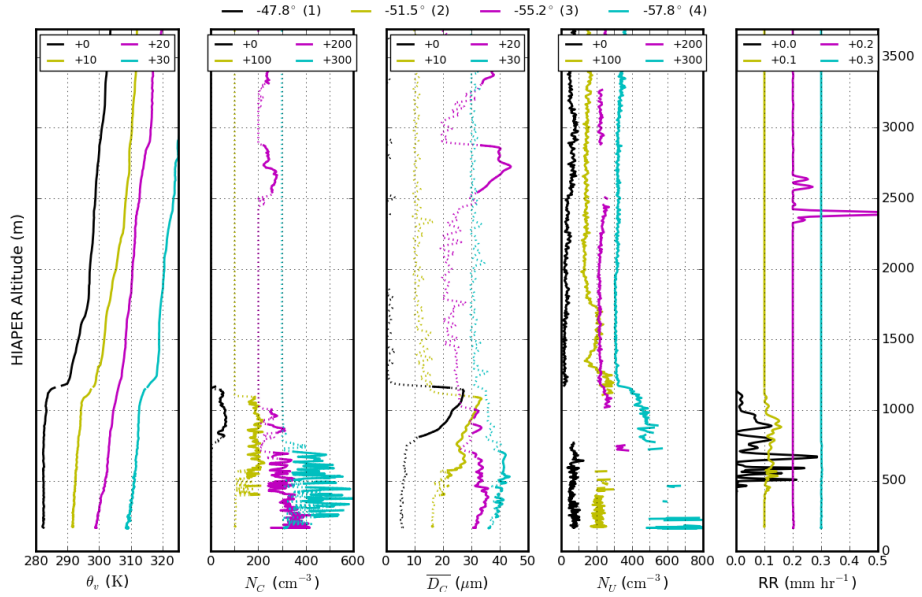

Figure 5. Profiles of microphysics variables within and above the boundary layer for RF06. From left: virtual potential temperature (θ_v, repeated for reference to other variables); CDP number concentration (N_C, masked where $\rho_L < 0.05\,g\,m^{-3}$); CDP mean diameter ($\overline{D_C}$, masked where $\rho_L < 0.05\,g\,m^{-3}$); UHSAS number concentration (N_U; masked where $\rho_L > 0.01\,g\,m^{-3}$); and 2DC-derived rain rate (RR).

ACPD
15, 25503–25545, 2015

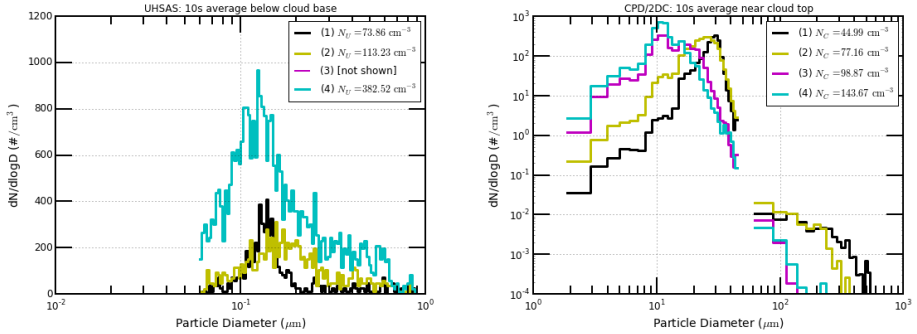

Figure 6. Left: Particle size distribution (10 s averages) for aerosol observed below cloud base by the UHSAS. Right: cloud droplets observed by the CDP at cloud top, and drizzle drops observed by the 2DC near cloud base (also 10 s averages; note logarithmic *y* scale).

ACPD
15, 25503–25545, 2015

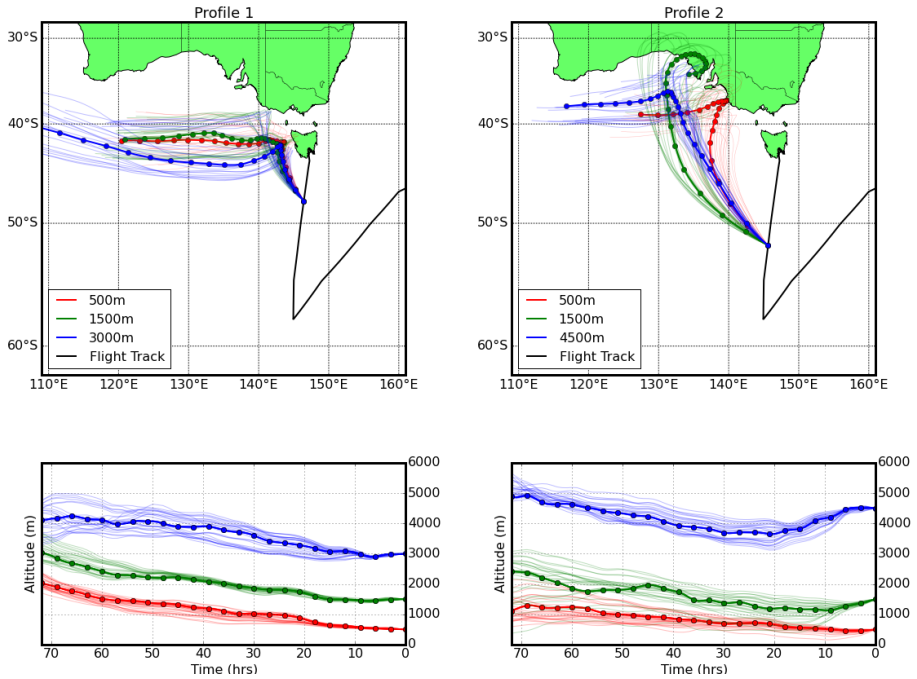

Figure 7. 72 h HYSPLIT Back trajectory ensembles for profiles 1 and 2, with arrival heigths indicated in the legends. Back trajectories were calculated with 1° horizontal resolution Global Data Assimilation System meteorological data, with the different ensemble members representing perturbations from the aircraft location of 1 grid space in the horizontal and 0.01 σ (about 250 m) in the vertical. The "deterministic" trajectories are heavier weighted lines with three hourly circle markers for each ensemble.

ACPD
15, 25503–25545, 2015

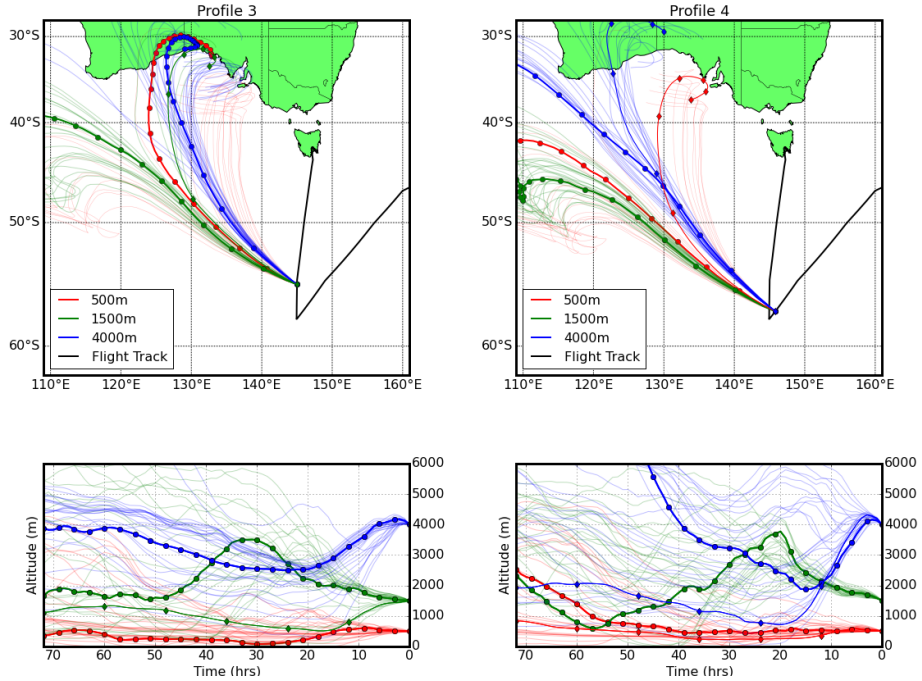

Figure 8. As for Fig. 7, but for profiles 3 and 4. In this figure some additional ensemble members, which represent substantially different airmass histories from the "deterministic" trajectories, have been highlighted with 12 hourly diamond markers.

ACPD
15, 25503–25545, 2015

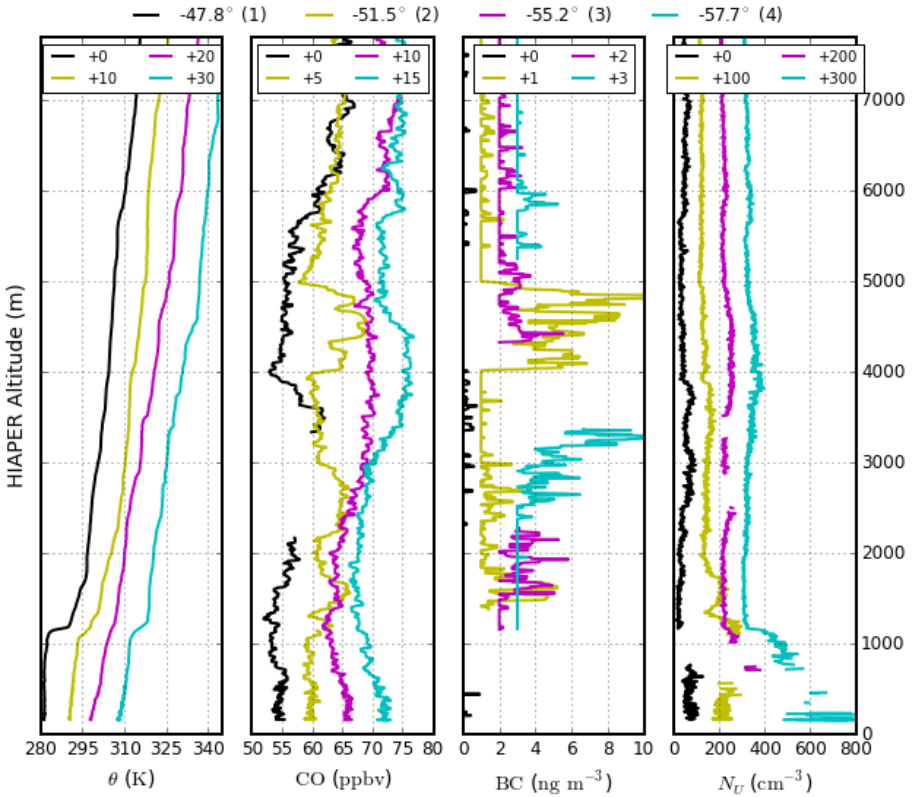

Figure 9. Trace gas and aerosol profiles for comparison flight RF06. From left: potential temperature (θ); Aerolaser VUV resonance fluorescence carbon monoxide concentration (CO); SP2 black carbon (BC) mass concentration; and UHSAS number concentration (N_U; missing for in-cloud conditions). Note that the y scale is different to Figs. 4 and 5, and now shows the entire vertical extent of the profiles.

ACPD
15, 25503–25545, 2015

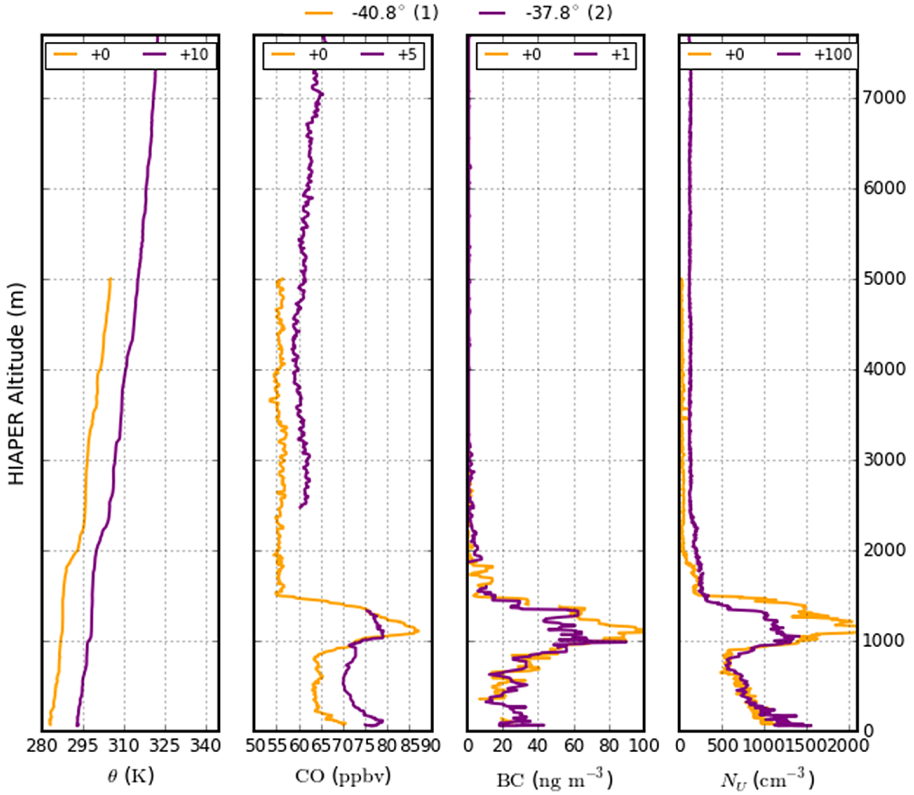

Figure 10. As for Fig. 9, but for RF07, showing a clear example of a polluted plume over the Bass Straight to the south of Melbourne. Note different x scales for CO, BC and N_U compared to Fig. 9.

ACPD
15, 25503–25545, 2015